Polymer 185 (2019) 121931

Contents lists available at ScienceDirect

Polymer

journal homepage: http://www.elsevier.com/locate/polymer

Alkaline stability of model anion exchange membranes based on poly (phenylene oxide) (PPO) with grafted quaternary ammonium groups: Influence of the functionalization route

R.-A. Becerra-Arciniegas [a,c], R. Narducci [a], G. Ercolani [b], S. Antonaroli [b], E. Sgreccia [a], L. Pasquini [c], P. Knauth [c], M.L. Di Vona [a,*]

[a] University of Rome Tor Vergata, Dep. Industrial Engineering, International Associated Laboratory: Ionomer Materials for Energy, 00133, Roma, Italy
[b] University of Rome Tor Vergata, Dep. Chemical Sciences and Technologies, 00133, Roma, Italy
[c] Aix Marseille Univ, CNRS, MADIREL (UMR 7246), International Associated Laboratory: Ionomer Materials for Energy, Campus St Jérôme, 13013, Marseille, France

ARTICLE INFO

Keywords:
Degradation
Mechanical properties
Ionic conductivity
DFT calculations

ABSTRACT

We study the effect of pendent methyl groups on the alkaline stability of model anion exchange polymers based on poly(2,6-dimethyl-1,4-phenylene)oxide (PPO) with grafted trimethylammonium groups. The polymer backbone is modified varying the synthesis procedure: by the bromination route, the ionomeric ammonium groups are inserted on the structural methyl group of PPO (Br-PPO-TMA), while by the chloromethylation route the ammonium groups are attached in the *ortho*-position to the methyl group of PPO (Cl-PPO-TMA). The properties of the membranes are studied by NMR and FTIR spectroscopy, thermogravimetry, water uptake, mechanical tensile tests, small-angle X-ray scattering (SAXS) and impedance spectroscopy. SAXS analysis indicates a better nanophase separation for Cl-PPO-TMA, which is consistent with a slightly larger water uptake and ionic conductivity. The properties of the two polymers are also compared before and after the aging in 2 M NaOH at 80 °C for different times. The thermogravimetric analysis shows the loss of the ammonium groups and the backbone ether cleavage after alkali treatments. The samples prepared by the bromination route show a higher stability of ionic conductivity, presumably due to a reduced alkaline attack of the ammonium groups, although DFT calculations do not show major differences of thermodynamic and kinetic reaction parameters. After alkaline treatment, the mechanical properties are more degraded for the Br-PPO-TMA compound. The decreased mechanical properties can be attributed to a reduction of the average chain length of PPO by alkaline scission of the ether links. Both synthesis routes have advantages and disadvantages, but the higher reproducibility and the better mechanical properties of samples prepared by chloromethylation are considered preponderant benefits.

1. Introduction

Hydroxide-conducting ionomers are promising materials for anion exchange membrane fuel cells (AEMFC) [1–5]. An important potential advantage of this technology is that less expensive and more abundant metals than platinum can be used to catalyze the oxygen reduction reaction in basic conditions, including, among others, nickel, iron, silver, carbon nanotubes supporting metal nanoparticles [6], or graphene with Fe/Co active sites [7]. Like in the case of the more prominent proton exchange membranes (PEM) [8–10], the hydroxide ion conduction occurs through percolating aqueous channels [11]. However, the nanophase separation is less efficient than in PEM, because ammonium groups are less hydrophilic, but mobile side chains can assist the hydrophilic/hydrophobic phase separation [12].

Unfortunately, the insufficient stability of hydroxide-conducting ionomer membranes in alkaline medium is a challenge for the large-scale implementation of AEMFC [13–15]. The nucleophilic attack by hydroxide ions involves two principal degradation mechanisms [5,16,17]: the second-order nucleophilic substitution (S_N2) leads mainly to the formation of an alcohol, whereas elimination reactions give a double bond. The S_N2 substitution on a benzylic derivative is difficult to prevent and depends *inter alia* on the strength of the nucleophile and on the concentration of both nucleophile and benzylic ammonium moiety. The so-called Hofmann elimination (E2) can occur only in the presence of a

* Corresponding author.
E-mail address: divona@uniroma2.it (M.L. Di Vona).

https://doi.org/10.1016/j.polymer.2019.121931
Received 26 July 2019; Received in revised form 30 September 2019; Accepted 19 October 2019
Available online 23 October 2019

hydrogen atom adjacent to the ammonium group (β-position). In case of important steric hindrance, the first-order elimination reaction (E1) can take place [13]. The AEM processing and handling is generally difficult and the degradation is often accompanied by the deterioration of the mechanical properties. Small changes in the polymeric structure can affect the performances in an important way [18–20].

The synthesis of AEM is generally conducted by introducing a halo-alkyl group on the pristine polymer followed by the quaternization reaction with a tertiary amine. Poly(2,6-dimethyl-1,4-phenylene)oxide (PPO) is a versatile backbone for polymeric electrolytes. The presence of activated aromatic rings together with allylic portions, due to methyl groups on the aromatic moieties, allows different functionalization strategies. The two main routes, bromination and chloromethylation, present advantages and disadvantages from the synthetic point of view. The radical bromination of the allyl moieties with *N*-bromosuccinimide (NBS) is the most used reaction to obtain a bromomethylated derivative that is easily transformed in ammonium groups. The advantages of the bromination route are the short reaction time and the easy conversion into the aminated derivative, via a S_N2 mechanism, due to the very good leaving group (Br). The degree of bromination (DBr) can be controlled varying the quantity of reagents (PPO and NBS) and the temperature. The disadvantages are the presence of radical species that can lead to undesired side reactions, such as cross-linking or oxidation, and some bromination of the aromatic ring.

The halo-methyl group can be also inserted via the chloromethylation reaction. This procedure can be nowadays conducted in a safe way, avoiding the initially used toxic and dangerous reagents [21,22]. Chloromethylation has the advantage to present a high reproducibility, because the degree of chloromethylation (DCM) can be carefully controlled varying the reaction time. The main disadvantages are a longer chloromethylation reaction and a lower amination yield in the studied conditions, because chlorine has a lower leaving group ability.

In this work, we study the influence on the alkaline stability of AEM using PPO as base polymer and anchoring the quaternary ammonium groups in different positions through the chloromethylation *vs* the bromination route. The two samples are studied and compared from the point of view of mechanical, thermal, conductivity and stability properties.

2. Experimental

2.1. Materials synthesis

Poly(2,6-dimethyl-1,4-phenylene)oxide (PPO, MW = 50000 g/mol) and all reagents were reagent-grade purchased from Sigma-Aldrich.

AEM were obtained in two steps: i) through either chloromethylation or radical bromination, and ii) by subsequent nucleophilic substitution (quaternization) [23].

2.1.1. Chloromethylation of PPO (Cl-PPO)

The chloromethylation synthesis was adapted from Refs. [24–27]. The reaction was carried out under nitrogen atmosphere. PPO (5.04 g, 42 mmol) was dissolved in 500 mL chloroform and 198 mmol (5.98 g) of paraformaldehyde was added and stirred during 1 h. Then 4.2 mmol (0.46 mL) of $SnCl_4$ was added at room temperature. A solution of trimethyl-chlorosilane (198 mmol, 25 mL) in chloroform was introduced dropwise during 2 h. The temperature was increased and kept at 40 °C. The chloromethylation degree (DCl) was controlled as function of the time.

To obtain a DCl of 0.3, 0.42, and 0.54, the reaction was kept at 45 °C for 17 h, 20 h and 25 h. After this time, the temperature was decreased and 150 mL of methanol added at RT until complete precipitation. The formed Cl-PPO was washed with methanol and dried at 60 °C for 48 h. The products were dissolved in $CDCl_3$ and analyzed by ^{1}H NMR.

2.1.2. Bromination of PPO (Br-PPO)

The radical bromination reaction was carried out under nitrogen atmosphere. PPO (42 mmol, 5.04 g) was dissolved in 140 mL of chlorobenzene. Then 2.1 mmol (0.51 g) of benzoyl peroxide (BPO) and 17.5 mmol (2.93 g) of *N*-Bromosuccinimide (NBS) were added under vigorous stirring; the temperature was increased and kept around 85 °C. After 1.5 h, a second amount of (2.93 g, 17.5 mmol) of NBS was introduced. The addition of NBS in two portions had the finality to maintain Br_2 at a low concentration and to decrease the quantity of aryl substitution. After 3.5 h, the mixture was cooled to ambient temperature. The product was precipitated adding 100 mL ethanol and the yellow solid was filtered. To purify the solid, it was dissolved in chloroform and then precipitated with methanol. The purification was repeated 3 times. The powder was dried during 24 h at 60 °C. Using this procedure, a bromination degree DBr = 0.24 in the benzylic position (0.08 in the aryl position) was obtained. The quantity of bromine substitution of methyl groups was controlled by changing the molar ratio PPO/NBS. To obtain a DBr = 0.30 in the benzyl position (0.12 in aryl position), we changed the molar ratio PPO/NBS = 1.0, other quantities remained constant.

2.1.3. PPO quaternization

Cl-PPO and Br-PPO were dissolved in 1-methyl-2-pyrrolidinone (NMP) and reacted with an excess of trimethylamine (TMA): the molar ratio of TMA (31–35 wt% in ethanol, 4.2 M) was 2:1 with respect to the amount of polymer (Table 1). Typical quantities of reactants employed in the reactions were: for the chloromethylation route, 3.73 mmol (0.50 g) of Cl-PPO (DCl = 0.3) and 7.46 mmol (1.84 mL) of TMA in 40 mL NMP; for the bromination route, 5.1 mmol (0.7 g) of Br-PPO (DBr = 0.3) reacted with 10.2 mmol (2.3 mL) of TMA in 50 mL NMP. The reactions were carried out during 48 h at 70 °C in dry conditions. After this time, the excess of TMA was eliminated by heating the solution under reduced pressure at 80 °C for 2 h. The solution was directly used for the casting procedure. Small portions were dried, dissolved in DMSO-d_6 and analyzed by ^{1}H NMR spectroscopy. The degree of functionalization (DF) was measured by NMR spectroscopy.

2.1.4. Membrane casting

The AEM were cast from a Petri dish by drying the NMP solution with a concentration around 0.3 g/25 mL in an oven at 95 °C. The membranes were purified again by immersion in distilled water at 60 °C during 2 days.

Table 1
Degree of functionalization (DF) of halogenated precursors, IEC of membranes, reaction yields, and Degree of unreacted (DU) halogen-methylated precursor obtained by NMR.

Samples	DF	IEC theory [a] (meq/g)	IEC titration [b] (meq/g)	IEC NMR [c] (meq/g)	Reaction Yield [d] (%)	DU
Cl-PPO-TMA	0.30	2.1	0.8	–	38	0.19
Cl-PPO-TMA	0.42	2.8	1.6	1.6	57	0.17
Cl-PPO-TMA	0.54	3.4	2.2	–	64	0.20
Br-PPO-TMA	0.24	1.9	1.6	1.7	84	0.04
Br-PPO-TMA	0.30	2.2	1.9	–	86	0.04

[a] Calculated from eq. (3).
[b] Obtained from Mohr titration.
[c] Calculated from DF obtained by NMR and eq. (3).
[d] Obtained from IEC(titration)/IEC(theory).

2.2. Characterization techniques

2.2.1. NMR spectroscopy

^{1}H NMR spectra were recorded with a Bruker Avance 400 spectrometer operating at 400.13 MHz using deuterated solvents (DMSO-d_6, $CDCl_3$). Chemical shifts (ppm) were referenced to tetramethylsilane (TMS).

2.2.2. FTIR spectroscopy

FTIR spectra were recorded in transmission mode in the range of 4000–400 cm^{-1} using a spectrometer PerkinElmer Spectrum 100. Spectra were normalized against a background spectrum.

2.2.3. Thermogravimetric analysis (TGA)

High-resolution TGA analysis was performed with a TA Q500 apparatus. The samples were contained in Pt sample holders. The experiments were made in air or in argon flux between 50 and 600 °C. The maximum heating rate was 3 K/min.

2.2.4. Tensile stress-strain measurements

The mechanical analysis was made in a traction machine ADAMEL Lhomargy DY30 at room temperature and ambient humidity ((50 ± 10) % RH) and also at full humidification.

2.2.5. Ion exchange capacity (IEC) by Mohr titration

The chloride form was obtained by treating the membranes in 1 M NaCl solution during 48 h. The membranes were then washed carefully with bi-distilled water to remove the excess Cl^-. The Cl^- anions contained in the membranes were exchanged with SO_4^{2-} treating them in 1 M Na_2SO_4 solution. This solution was titrated using 0.02 M $AgNO_3$ and as indicator K_2CrO_4. The indicator was prepared dissolving 1 g of K_2CrO_4 in 20 mL of water.

2.2.6. Ion conductivity

The membranes in OH^- form were obtained by treatment in 2 M NaOH solution during 48 h then washed in distilled water under nitrogen. The instrument employed was a VSP-300 (Biologic science instruments) in PEIS mode (Potentiostatic Electrochemical Impedance Spectroscopy). This analysis was performed between 1 Hz and 6 MHz with a signal amplitude of 20 mV inside a hermetically closed Swagelok cell with stainless steel electrodes in order to limit as much as possible the formation of HCO_3^- ions by reaction with atmospheric CO_2 [28]. The resistance of the membranes at 25, 40, 60 and 80 °C was obtained from a Nyquist plot by non-linear least-square fitting using an equivalent circuit composed of a series arrangement of two resistance-constant phase elements in parallel. The ionic conductivity was calculated using the resistance R, the membrane thickness d, typically 60–80 μm, and the electrode area A = 0.28 cm^2:

$$\sigma = d / (A*R) \quad (1)$$

2.2.7. Water uptake

The membranes in OH^- form were dried over P_2O_5 under nitrogen during 48 h and the mass of the dry samples was measured (m_{dry}). The samples were then hydrated in deionized water during 48 h under nitrogen and the mass of fully humidified membranes was obtained (m_{wet}). The water uptake (in %) was calculated from the equation:

$$WU = 100*\frac{m_{wet} - m_{dry}}{m_{dry}} \quad (2)$$

2.2.8. Stability tests

Small membrane samples were treated in 2 M NaOH solution at 80 °C during a determined period of time from 24 h to 120 h. After the treatment, they were washed carefully with ultrapure water under nitrogen to remove the excess of NaOH. The membranes were finally hydrated in ultrapure water during 40 min and their ionic conductivity was determined. Aged membranes were also characterized by FTIR and NMR spectroscopies, mechanical tests and titration.

3. Results and discussion

3.1. Synthesis

The pathways for the synthesis of Cl-PPO-TMA and Br-PPO-TMA are reported in Fig. 1.

Cl-PPO is synthetized using non-toxic reagents: the dangerous chloromethylating agent is formed in situ and quenched at the end of the reaction by adding ethanol [21]. It is possible to avoid side-reactions, such as the formation of the cross-linked polymer via the Friedel-Crafts reaction, by carefully adjusting the reaction temperature and the concentration of the reagents. The degree of chloromethylation is controlled through the reaction time with good reproducibility as shown in Fig. 2.

Samples with a degree of chloromethylation between 0.6 and 0.92 show a high water solubility due to the high Ionic Exchange Capacity (IEC). They were abandoned for this reason.

The radical bromination reaction is carried out using NBS as source of bromine [29,30]. This reaction is known as benzylic bromination or Wohl–Ziegler reaction [31] and occurs in the presence of a radical initiator (BPO). The reaction is very fast, and the experiments are less reproducible than the chloromethylation. However, the degree of bromomethylation is controlled by the ratio between the reagents (Fig. 3).

The substitution in the aromatic ring can be further decreased or avoided by increasing the reaction temperature. However, increasing the temperature above 100 °C leads to secondary reactions, such as crosslinking.

3.2. IEC

Table 1 shows a comparison of the calculated IEC, assuming a quantitative reaction of TMA with halogenated precursors with various degrees of functionalization (DF), and the IEC measured by Mohr titration.

The relation between DF and the theoretical IEC (in meq/g) is given by equation (3) [32]:

$$DF = \frac{IEC \times M_{(PPO-CH_2)}}{1 - IEC \times M_{(TMA)}} \quad (3)$$

where DF, $M_{(PPO-CH_2)} = 134$ g/mol and $M_{(TMA)} = 59$ g/mol are the degree of functionalization, the equivalent mass of the polymer and the molar mass of TMA respectively.

The ratio between the theoretical IEC and the experimental IEC values gives the reaction yield of the amination reaction. In all cases, the molar ratio between TMA and halogen-methylated groups was higher than 2. The yields increase with the precursor DF, in agreement with second order kinetic laws. There are notably higher reaction yields by the bromination route, which can be attributed to a lower steric hindrance of the precursor and the better leaving group ability of Br.

As shown in Fig. 4, it is not possible to observe directly in the NMR spectra the peaks ascribed to the unreacted halogen-methylated groups due to the overlap of the signal of $–CH_2X$ and $–CH_2N^+(CH_3)_3$ moieties. However, an estimation may be obtained comparing the area of the total methylene groups with the area of methyl moieties linked to ammonium atom $–N^+(CH_3)_3$. In the case of Cl-PPO-TMA with DF = 0.42 the ratio between the real and nominal values of signal h (2.71 vs 4.50) gives a conversion of 60% (Fig. 4) in good agreement with the data obtain by titration. Considering the initial DF = 0.42 one may assign for the Cl-PPO-TMA repeat units n = 0.58, x = 0.25, y = 0.17 (see Fig. 1). The other values (DU) reported in Table 1 are assigned in the same way.

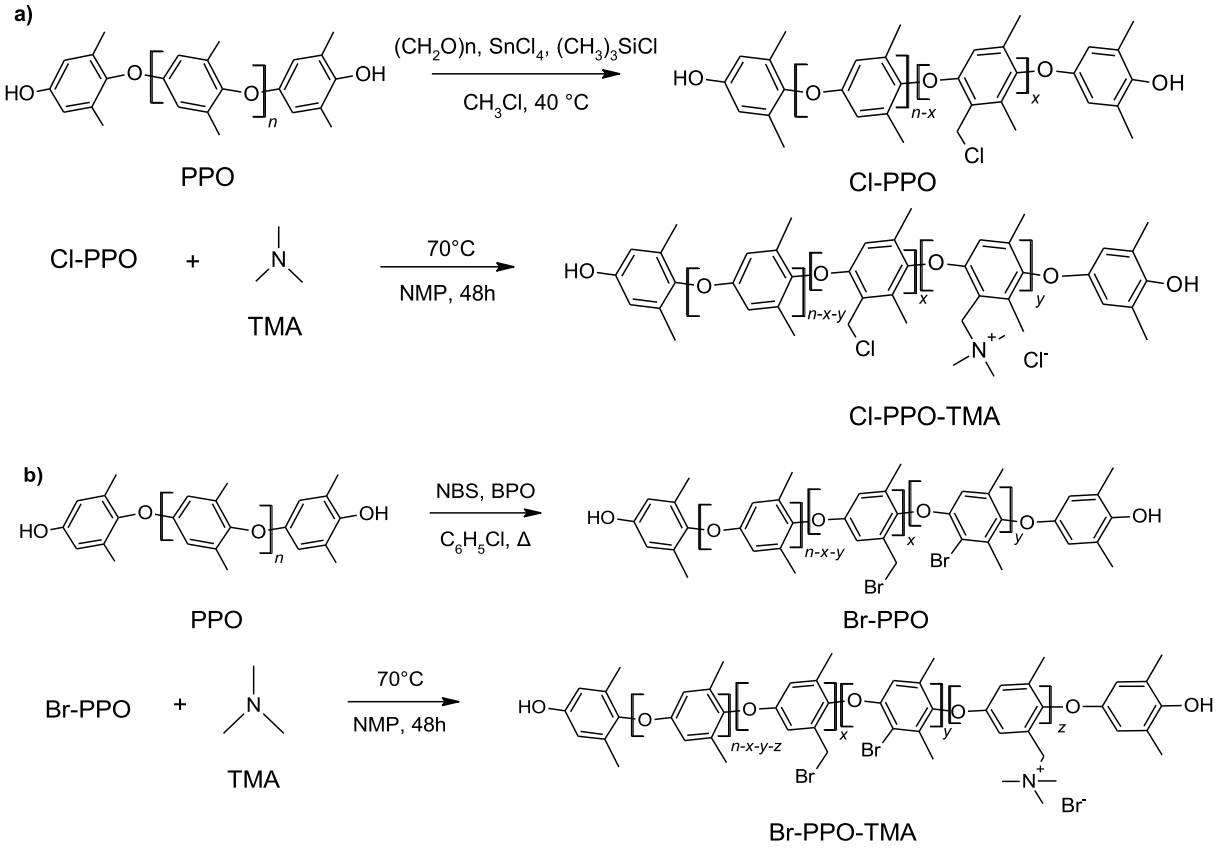

Fig. 1. Reaction pathways for the AEM synthesis via quaternization of a) chloromethylated and b) brominated precursors.

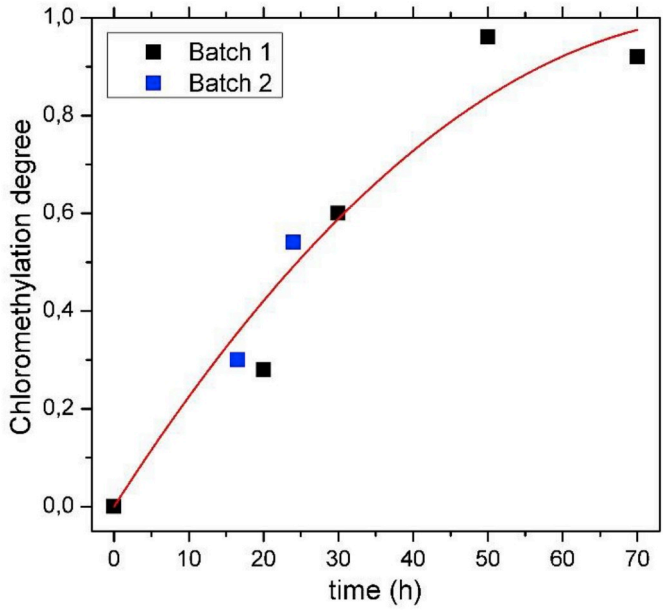

Fig. 2. Chloromethylation degree of PPO as function of the reaction time. (For interpretation of the references to color in this figure legend, the reader is referred to the Web version of this article.)

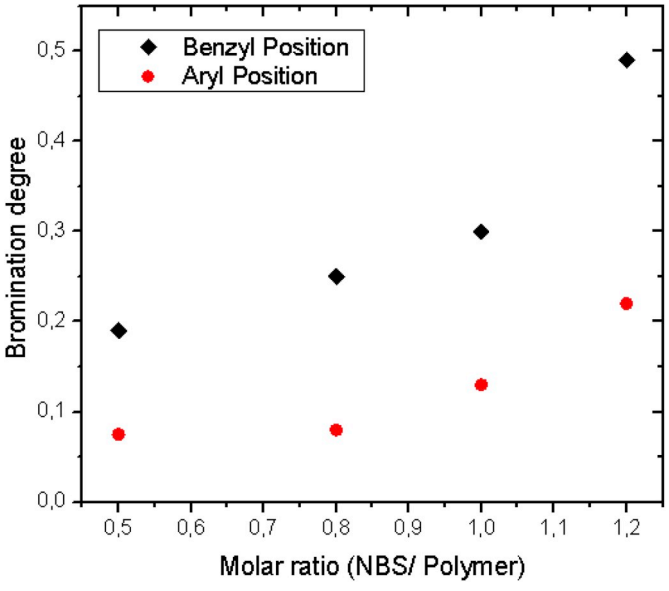

Fig. 3. Bromination degree of PPO in the different positions as function of molar ratio NBS/Polymer.

3.3. Water uptake

The water uptake and hydration numbers of membranes in hydroxide form at 20, 60 and 90 °C (Fig. 5) are generally quite low; a relatively small increase is especially observed at 90 °C. The WU is correlated with the IEC, but the dependence is only modest. The WU of Cl-PPO-TMA appears slightly higher than that of Br-PPO-TMA. The swelling behavior was measured for the Cl-PPO-TMA sample with IEC = 1.6 meq/g at 20, 45, 60, and 90 °C for 24 h in water and gave the following values: 17, 28, 40, and 40% respectively.

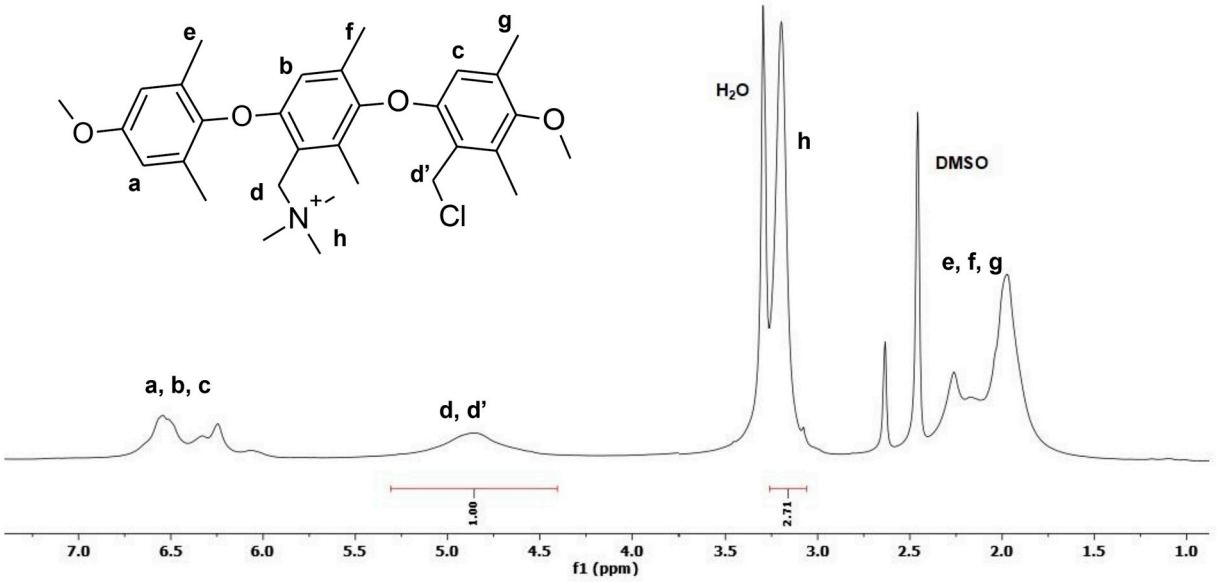

Fig. 4. ^{1}H NMR spectrum of Cl-PPO-TMA with DF = 0.42.

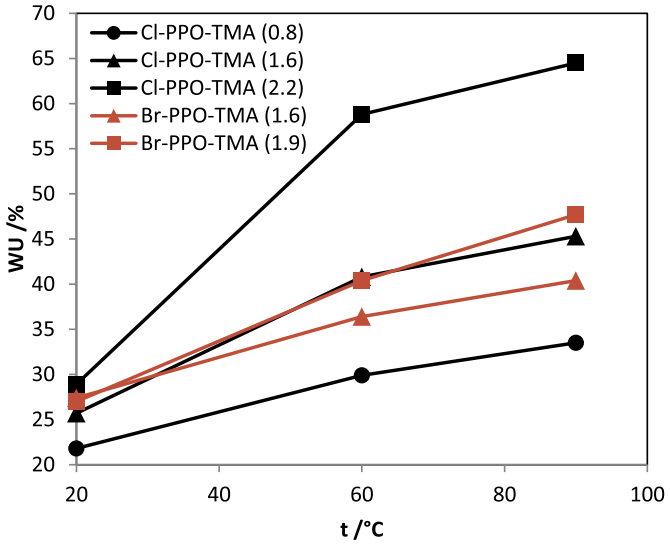

Fig. 5. Water uptake (WU) values at different temperatures.

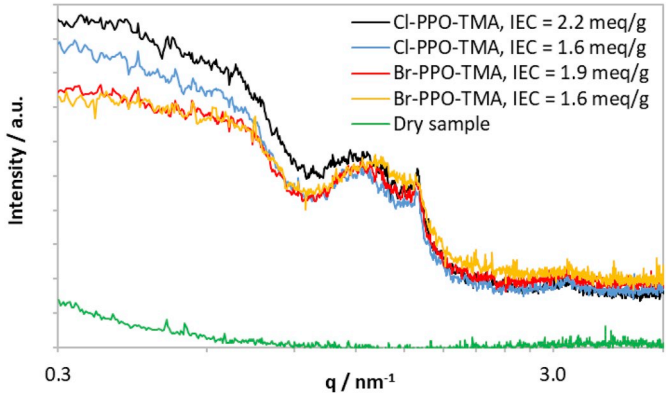

Fig. 6. SAXS patterns of fully humidified samples with various IEC and comparison with a dry sample.

3.4. Small angle X-ray scattering

The SAXS patterns of fully humidified samples (Fig. 6) show a broad peak around a scattering vector $q = 1.2\,\mathrm{nm}^{-1}$. This "ionomer peak" is attributed to the hydrophilic-hydrophobic nanophase separation [33–37]. In fact, dry samples do not show this X-ray scattering peak (green line in Fig. 6). The large width of the peaks indicates a weak separation between hydrophobic and hydrophilic domains. The peak position shifts to slightly larger q for Br-PPO-TMA. The characteristic inter-domain spacing or separation length between ion-rich domains d can be calculated from the q values corresponding to the ionomer peak, according to the equation:

$$d = \frac{2\pi}{q} \tag{4}$$

Cl-PPO-TMA shows a slightly longer separation distance (d = 5.2 nm) than Br-PPO-TMA (d = 4.8 nm), indicating a better hydrophilic−hydrophobic nanophase separation for Cl-PPO-TMA, probably because the partial bromination of aryl groups in Br-PPO-TMA introduces hydrophobic moieties near the hydrophilic ammonium groups. The sharp little peak at $q = 1.6\,\mathrm{nm}^{-1}$ indicates some long-range order with d ≈ 4 nm, which is not yet fully understood.

3.5. Hydroxide ion conductivity

The ionic conductivity for various IEC is shown in Table 2 together with the calculated activation energies. For Cl-PPO-TMA samples, the ionic conductivity actually decreases when the IEC increases above 2 meq/g, as previously reported in the literature [21]; instead the conductivity increases with the IEC for Br-PPO-TMA.

The average activation energy of (0.10 ± 0.02) eV is consistent with hydroxide ion conduction in an aqueous medium [38].

Table 2
Hydroxide ion conductivities and activation energies of AEM.

Samples	IEC /(meq g^{-1})	σ / (mS cm^{-1})				Activation Energy / eV
		25 °C	40 °C	60 °C	80 °C	
Cl-PPO-TMA	1.6	4.6	5.6	7.0	10.6	0.10
Cl-PPO-TMA	2.2	3.7	4.8	5.9	-	0.11
Br-PPO-TMA	1.6	3.9	4.4	6.3	9.3	0.12
Br-PPO-TMA	1.9	4.5	5.3	6.3	-	0.08

4. Stability tests: characterization of ionomer degradation

4.1. FTIR analysis

Fig. 7 shows the spectra of Br-PPO-TMA and Cl-PPO-TMA before and after 3 days in KOH. Characteristic absorptions of PPO are present in the spectra at 1610 and 1470 cm^{-1}, ascribed to the stretching vibration of the phenyl groups, at 1188 and 1310 cm^{-1}, due to the symmetrical and asymmetrical stretching vibrations of the C–O–C backbone, and at 1030 cm^{-1} ascribed to the methyl rocking vibrations. The main differences between the pristine and aged samples are underlined in Fig. 7. For Br-PPO-TMA (Fig. 7a) it is possible to observe at 1692 cm^{-1} a peak in the typical range of carboxylic acids that can be due to the oxidation products of methyl groups on the aromatic ring [39,40]. A small peak at 1240 cm^{-1} can be ascribed to the C–H stretching vibration of aldehydes due to the oxidation of methanol formed by the S_N2 reaction of ammonium groups with OH^-. Also, the absorption at 1188 cm^{-1}, due to the stretching of the C–O–C moieties, seems changed in the aged compound and a new peak at 1170 cm^{-1} appears in the region of phenol absorption indicating the degradation of the backbone. The CH_3 groups of trimethylammonium moieties are expected to absorb in the region 3100-3020 cm^{-1} and they overlap in a large part with the methyl groups of PPO [41]. The reduction of the peak at 3040 cm^{-1} in the aged sample and the low intensity of the OH band around 3400 cm^{-1} can be related to the loss of hydrophilic ammonium groups. The effect of the degradation can be also seen at 1095 cm^{-1}, corresponding to asymmetric C–N stretching, reduced in the aged compound [25,42,43]. Less changes can be observed in the spectra in Fig. 7b between pristine and aged Cl-PPO-TMA. The main differences are the peak at 1267 cm^{-1} occurring in the region of C–O–C vibrations, and the peak at 740 cm^{-1}, present in the pristine membrane, attributed to the stretching vibration of the C–Cl bond of unreacted chloromethyl groups. A lower intensity of the OH band around 3400 cm^{-1} can be ascribed to the loss of hydrophilic ammonium groups in the aged ionomer.

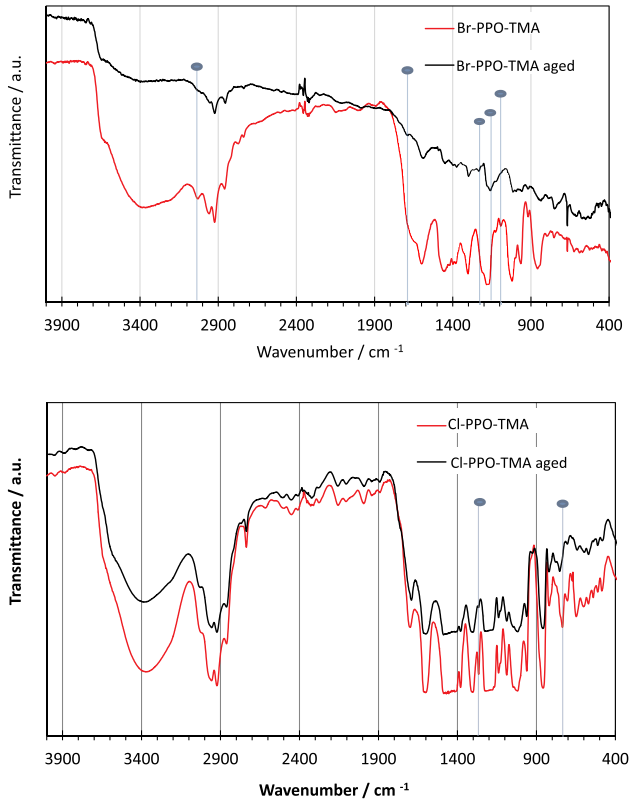

Fig. 7. FTIR spectra of pristine and aged: a) Br-PPO-TMA; b) Cl-PPO-TMA.

4.1.1. Thermogravimetry

The thermal decomposition of poly(phenylene oxides) forms mainly low molecular mass chain fragments, partially with hydroxyl end groups. The decomposition mechanism of PPO was postulated to begin with the cleavage of the ether linkages [44]. The various decomposition products are not only the result of chain cleavage, but also of partial or complete removal of the pendent methyl groups before the main chain degradation. Other free radicals can combine to form a crosslinked polymer [44]. In inert atmosphere, the decomposition of poly(2, 6-dimethyl-1,4-phenylene oxide) is observed above 400 °C with a residue of about 30% remaining at 600 °C [44].

The thermograms of Cl-PPO-TMA samples (Fig. 8a) show an initial mass loss below 100 °C, which is related to the loss of water; it corresponds to about 5% for the pristine sample and 3% after alkaline treatment, showing that hydrophilic groups have been lost. The mass loss above 150 °C can be attributed to the loss of the quarternary ammonium groups, which continues to more than 300 °C. Similar decomposition temperatures were reported in various references [17,36, 37,45–47]. The mass loss corresponds to about 9% for the pristine sample; it is smaller, about 5%, after the alkaline treatment, which evidently removes quaternary ammonium groups. For the pristine sample, the shoulder at 380 °C in the derivative curve can be attributed to the removal of pendant methyl [44] and unreacted chloromethyl groups. Chlorobenzylated PPO should decompose at a higher temperature than bromobenzylated PPO (see below), due to the stronger C–Cl bond. The decomposition of the PPO backbone is observed with a maximum at 425 °C, in good agreement with literature data [45,48,49]. The decomposition temperature of the polymer backbone is quite similar to its parent polymer, indicating that the loss of the quaternary ammonium groups does not trigger the backbone degradation, as previously observed in other AEM [46,47]. The residue at higher temperature, particularly in inert gas atmosphere, is related to PPO impurities, as previously observed [48].

After the alkaline treatment, the PPO decomposition peak is shifted to lower temperatures (Fig. 8a). One can assume that the nucleophilic attack of the polymer main chain by OH^- ions leads to a decrease of the average chain length of PPO by cleavage of the ether bonds, leading to a lower decomposition temperature. In inert gas, the decomposition peak around 350 °C is very sharp, whereas in air a double peak is observed, indicating the presence of oxidation products (see above). The broad signal at 380 °C contains certainly various degradation products, such as hydroxymethyl groups, whereas the sharp peak at 415 °C is attributed to some partially cross-linked PPO.

The thermograms of Br-PPO-TMA are more complicated (Fig. 8b).

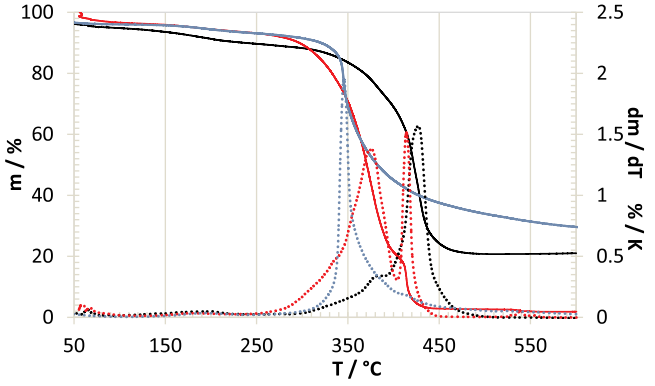

Fig. 8a. High-resolution thermograms of Cl-PPO-TMA. Pristine ionomer in air: black line. After 3 days in 2 M NaOH at 80 °C: red line in air, blue line in argon. Dotted lines: derivative curves. (For interpretation of the references to color in this figure legend, the reader is referred to the Web version of this article.)

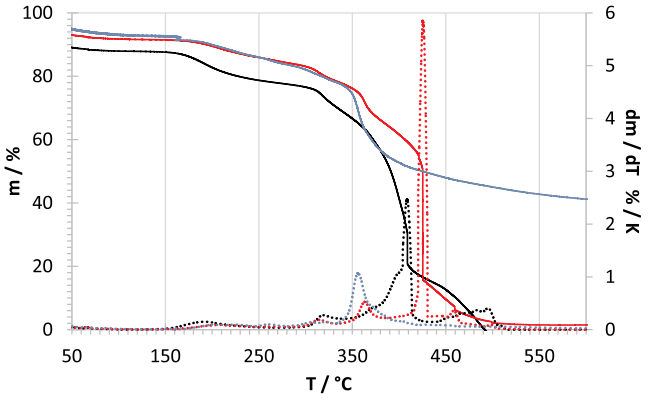

Fig. 8b. High-resolution thermograms of Br-PPO-TMA. Pristine ionomer in air: black line. After 3 days in 2 M NaOH at 80 °C: red line in air, blue line in argon. Dotted lines: derivative curves. (For interpretation of the references to color in this figure legend, the reader is referred to the Web version of this article.)

The loss of water below 100 °C amounts to 11% for the pristine vs. 7% for the aged ionomer, showing the loss of hydrophilic ammonium groups. The quaternary ammonium groups decompose between 150 and 300 °C; the mass loss is 11% for the pristine and 7% for the aged ionomer, evidently correlated with the water loss. The small peak at 320 °C (derivative curves) corresponds probably to the loss of bromine aryl substituents. Previous investigations show that the loss of Br substituents starts around 300 °C [45,46,49–51]. The peak corresponding to bromine substituents is shifted to about 260 °C in inert atmosphere; this strong effect has been reported previously [50]. The peak area decreases indicating a loss of aryl Br during the alkaline treatment. In air, the Br loss is confirmed, but the temperature is less changed. A shoulder and a small convoluted peak at 370 °C can be attributed to hydroxymethyl and methyl group removal. The decomposition of the main chain of the pristine ionomer occurs at a slightly lower temperature than for Cl-PPO-TMA (415 °C vs. 425 °C). After the degradation treatment in alkaline conditions, a shift to higher temperatures is observed in air, which might indicate cross-linking, e.g. by some carboxylic acid groups formed in situ by oxidation of methyl groups. The signals above 425 °C and up to 550 °C in air have been shown to correspond to oxidation products of PPO, especially of the methyl groups [48,50]; they are evidently reinforced by the partial aryl bromination.

4.1.2. NMR analysis

The spectra of the samples derived from the bromination route before and after the aging are reported in Fig. 9. Unfortunately, it is not possible to collect the spectrum of Cl-PPO-TMA after the aging, due to the poor solubility of the chloromethylated derivative, probably due to some cross-linking. The spectra in Fig. 9 are very similar except for new peaks around 1.25 and 3.6 ppm. The first peaks correspond to the degradation of the backbone with formation of alkyl moieties, also observed in the degradation of PPO [40,52]. The peaks around 3.6 ppm are assigned to *N*,*N*-dimethylbenzylamine or *N*-methylbenzylamine moieties, indicating an attack of OH^- on the methyl groups linked to the nitrogen. An estimation of the degradation yield can be made by the comparison with the area of peaks *d* (Fig. 9) due to the benzyl moieties.

Taking as a reference the aromatic PPO hydrogens (a,b,c) the degradation of the ammonium ion is around 25%, slightly lower with

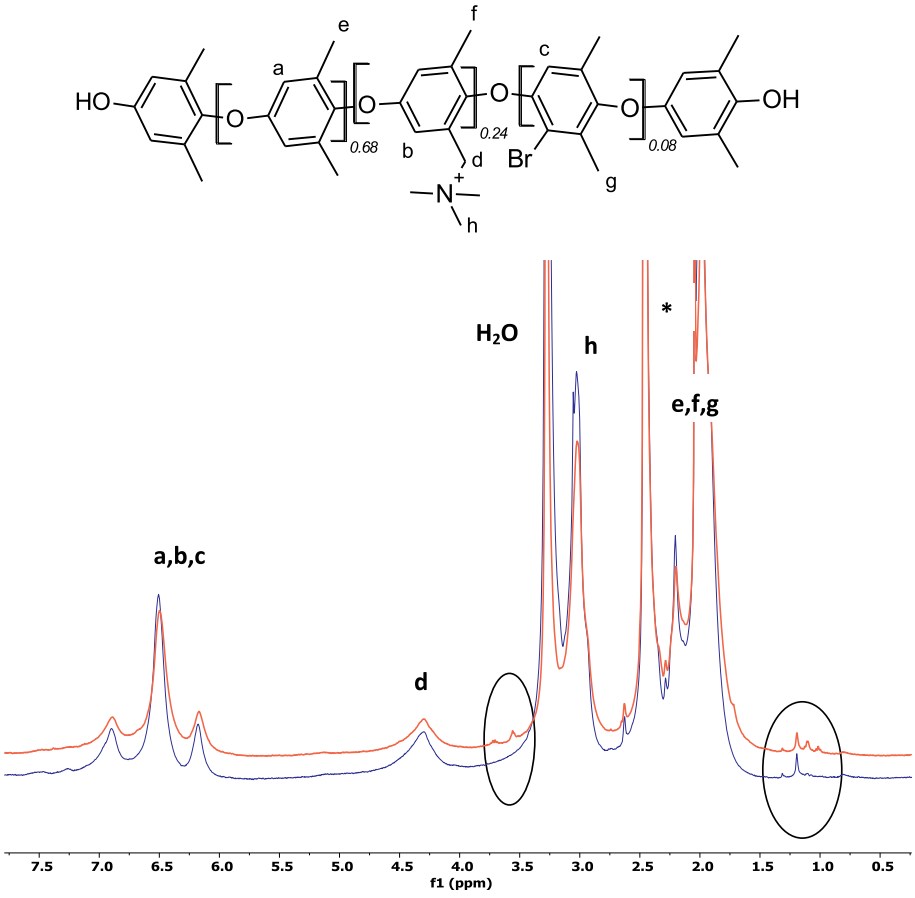

Fig. 9. ^{1}H NMR spectra of Br-PPO-TMA (DF = 0.24) pristine (blue line), and aged (red line). (For interpretation of the references to color in this figure legend, the reader is referred to the Web version of this article.)

respect to the thermogravimetric analysis. This estimation, in fact, does not consider the possible presence of the signals of benzylic alcohol groups, the main product of the degradation, that overlap in the same region.

4.1.3. Mechanical tests

Fig. 10 shows typical stress-strain tests for two AEM before and after the alkaline degradation ("Aged"). Both ionomers exhibit a very low tensile elongation at break compared to that of pristine PPO (50–60% [53]) and one can observe a further decrease of the elongation at break related to a loss of membrane ductility after the treatment in NaOH. The increased fragility of the membranes might be attributed to an attack of the ionomer backbone with a reduction of the average chain length. The lower ductility of Br-PPO-TMA vs Cl-PPO-TMA is confirmed by the handling experience showing that the former are more fragile. The greater fragility of Br-PPO-TMA might be related to some cross-linking by radical species formed in air or a better chain packing of the chloromethylated derivative [42].

Table 3 reports the mechanical properties at 50 and 100% RH. Young's modulus decreases consistently with increasing IEC, certainly due to a higher hydration, weakening the dipolar interactions among ionomer chains. The aged samples show therefore a high stiffness, but one can also observe a drastic decrease of the elongation at break, related to a loss of membrane ductility, and a reduction of the strength. The increased fragility of the aged membranes might be attributed to an attack of the ionomer backbone with a reduction of the average chain length. The lower elongation at break of Br-PPO-TMA vs Cl-PPO-TMA is confirmed by the handling experience showing that the former membranes are much more fragile [20]. At 100% RH, Young modulus and tensile strength are much reduced, due to the higher sample hydration.

4.1.4. Ionic conductivity

Fig. 11 shows the decrease of the ionic conductivity, taken as an indicator of membrane degradation, with the treatment time in NaOH. One notices that although the degradation after 1 day is relatively similar for AEM made using the chloromethylation and bromination routes, the brominated samples show a higher conductivity after 2 and 3 days, indicating a better long-time stability of Br-PPO-TMA. One notices also that the samples with a lower IEC have a higher conductivity after 2 and 3 days in NaOH. The determination of IEC by Mohr and acid-base titration after 72 h alkaline treatment of two samples with the same initial IEC (1.6 meq/g) confirms the more important loss of quarternary ammonium groups for Cl-PPO-TMA: IEC = 0.4 meq/g vs Br-PPO-TMA: IEC = 0.8 meq/g.

5. Discussion of the ionomer degradation

The degradation picture of Cl-PPO-TMA and Br-PPO-TMA is quite complex. Both undergo the quaternary ammonium degradation via a S_N2 mechanism. However the chloromethylated derivatives degrade more that the bromomethylated ones. The residual conductivity after 3 days is 15% for Cl-PPO-TMA and 38% for Br-PPO-TMA. On the contrary, the backbone degradation is more important for Br-PPO-TMA as observed by FTIR, thermogravimetry analyses, and mechanical tests. It was further confirmed by the evident brittleness of Br-PPO-TMA membranes after aging. The degradation of the backbone occurs mainly via the attack of OH^- on the ether linkage, and it is reduced when the electron density around the oxygens is high. Two factors may contribute to the enhanced stability of Cl-PPO-TMA: 1) the stabilization effect due to the electro-donating behaviour of the extra methyl group in Cl-PPO-TMA; 2) the destabilization effect of bromine linked to the aryl moieties in Br-PPO-TMA. Br is electron withdrawing for inductive effect (-I) and electro-donating for mesomeric effect (+R) with the last one predominant, leading to depleting the negative charge density on the oxygen of the ether linkage. Considering the –I effect of the ammonium group is very probable that the nucleophilic scissions of the ethers occurs on the aromatic portion bearing the quaternary group as shown in Fig. 12. This statement is supported by the stability of pristine PPO in alkaline conditions [53]. FTIR and thermogravimetry analyses indicate the presence of phenol moieties, the main product of ether breakage, and the presence of oxidation products, such as carboxylic acid and formaldehyde. The last ones may be obtained by the oxidation of aromatic methyl groups or benzylic alcohol, the product of the attack of OH^- on the ammonium ions. This reaction can be catalysed by the presence of the hydroxyl radical generated by the reaction of oxygen with the ylide form of PPO-TMA as reported in Ref. [52]. The free radicals formed during the oxidation of methyl groups can combine to form crosslinked polymers, as explained in the description of the thermogravimetry analyses. Regarding the by-product detected by NMR analysis at highfield it is believed to belong to ring opening reactions [45,54], although is unclear the exact degradation mechanism [45].

The S_N2 reaction of hydroxide anions on the benzylic carbon of Br-PPO-TMA and Cl-PPO-TMA in water was investigated by DFT calculations on the model compounds **1** and **2**, yielding the products **3** and **4**,

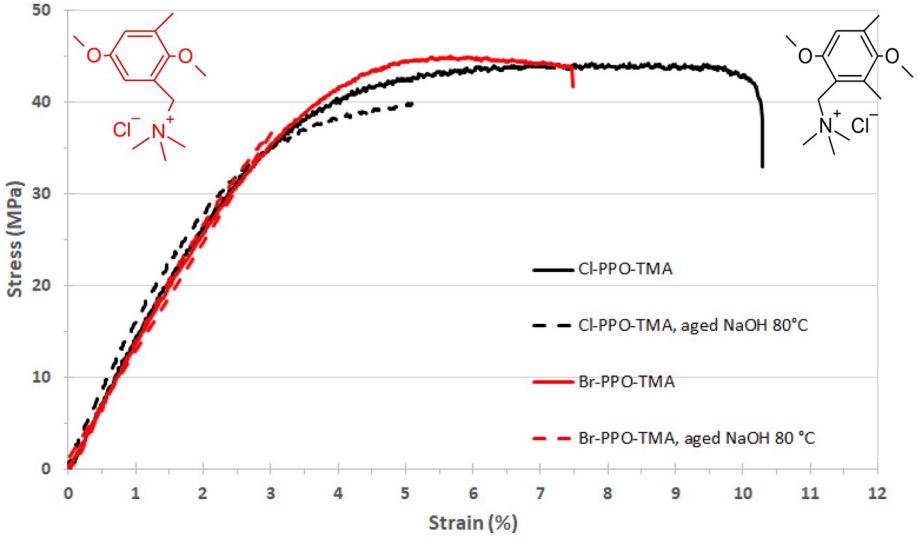

Fig. 10. Stress-strain tests at room temperature and ambient humidity (50 ± 10% RH) of AEM (chloride form, initial IEC = 1.6 meq/g) before and after aging in NaOH at 80 °C (72 h).

Table 3
Mechanical properties of AEM (Cl form) at RH = 50 and 100%.

	IEC/meq g^{-1}	Young's modulus/MPa		Tensile strength/MPa		Elongation at Break/%	
RH/%		50	100	50	100	50	100
Cl-PPO-TMA[a]	0.3	1660 ± 50	42 ± 2	5 ± 3			
Cl-PPO-TMA	1.6,1,	1426	880	44.1	19.4	10.3	4.3
Cl-PPO-TMA	2.2	1330	581	40.7	25.3	7.0	6.8
Br-PPO-TMA[a]	0.7	1530 ± 40	32 ± 4	2 ± 5			
Br-PPO-TMA	1.6	1324	952	44.7	32.6	7.5	6.0
Br-PPO-TMA	1.9	1250 ± 90	856	39.2 ± 0.3	23.0	5.5 ± 1.0	6.1

[a] Aged samples.

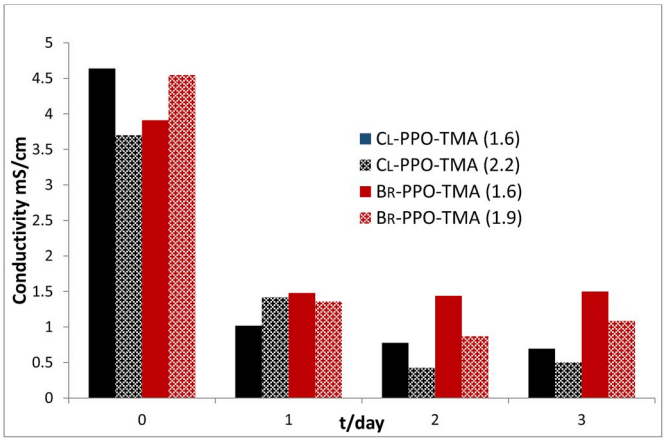

Fig. 11. Ionic conductivity of AEM as function of the treatment time in 2 M NaOH at 80 °C.

respectively (Fig. 13). Previous DFT studies on the degradation of tetralkylammonium ions can be found in the literature [55–58].

Geometry optimization and vibrational frequency calculations of reactants, transition states, and products were carried out with the APFD functional using the 6-311 + G(2d,p) basis set as implemented in the Gaussian 16 suite of programs [59]. The effect of water was taken into account by the Polarizable Continuum Model using the integral equation formalism (IEFPCM). Reaction and activation thermodynamic parameters refer to 1 mol/L standard state and 298 K.

For the reaction: **1** + OH^- → **3** + $N(CH_3)_3$, reaction and activation parameters were the following: $\Delta H^\circ = -25.8$ kcal/mol, $\Delta S^\circ = 14.4$ cal/mol K, $\Delta G^\circ = -30.1$ kcal/mol, $\Delta H^\ddagger = 10.2$ kcal/mol, $\Delta S^\ddagger = -20.0$ cal/mol K, $\Delta G^\ddagger = 16.1$ kcal/mol.

For the reaction: **2** + OH^- → **4** + $N(CH_3)_3$, reaction and activation parameters were the following: $\Delta H^\circ = -25.5$ kcal/mol, $\Delta S^\circ = 14.1$ cal/mol K, $\Delta G^\circ = -29.7$ kcal/mol, $\Delta H^\ddagger = 10.4$ kcal/mol, $\Delta S^\ddagger = -21.4$ cal/mol K, $\Delta G^\ddagger = 16.8$ kcal/mol.

The degradation reactions are thermodynamically downhill. A significant fraction of the Gibbs energy of activation is due to the entropic component as expected for a bimolecular mechanism. Both reaction and activation thermodynamic parameters are very similar for the two substrates suggesting that the methyl group in meta position in compound **1**, and the two methyl groups in *ortho* and *para* positions in compound **2** play a minor role in the reaction. However, not too much confidence should be put on exact figures because of the approximate treatment of solvation that does not take hydrogen bonding in due account, especially as far as the hydroxide ion is concerned.

Assuming that the loss of ammonium groups is a second order reaction, the reaction rate v should be proportional to the IEC and the OH^- concentration (k is the reaction constant):

$$v = \tilde{k} \cdot IEC \cdot [OH^-] \quad (5)$$

Concerning the hydroxide ion concentration dependence, the kinetic analysis must differentiate the rate of a reaction with the internal OH^-

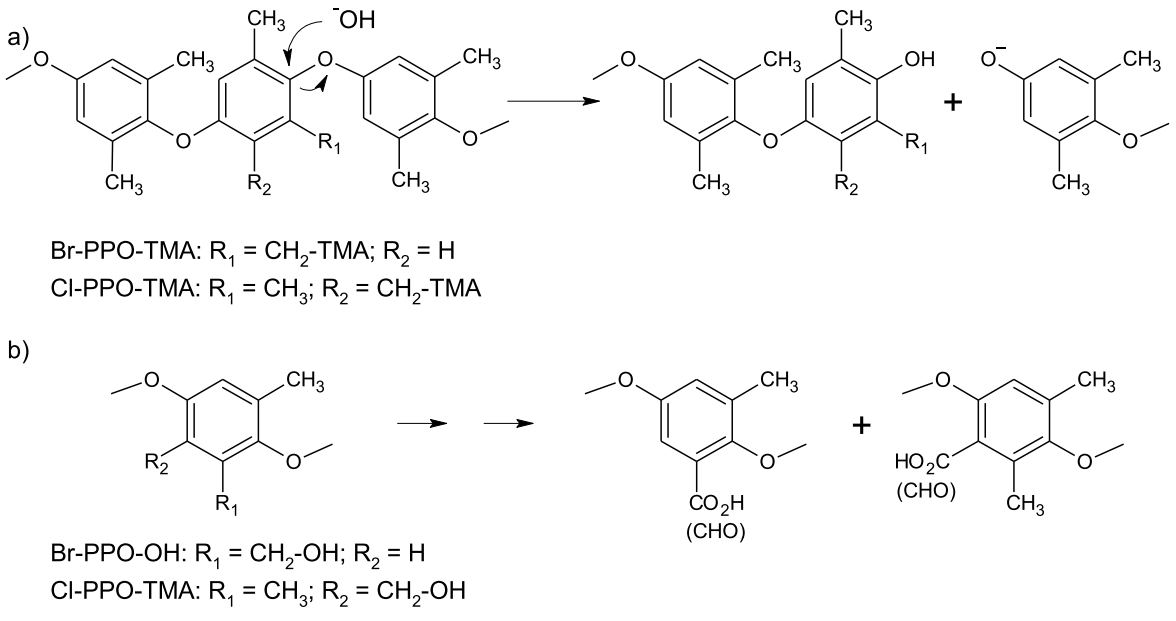

Fig. 12. Main backbone degradation pathways. a) ether breakage; b)oxidation.

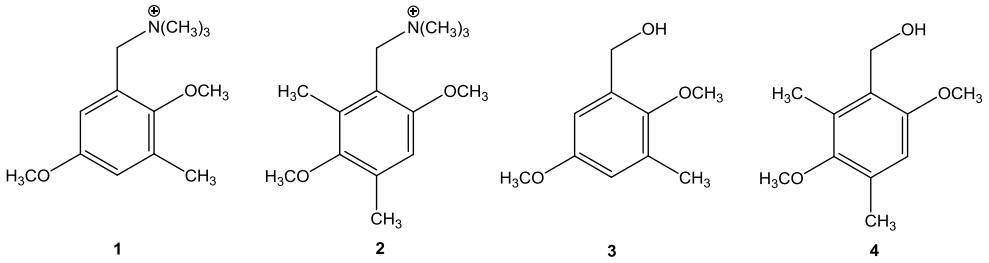

Fig. 13. Model reagents and products for DFT calculations.

ions, which are in equal concentration with the grafted ammonium counter-ions, from the treatment inside an external NaOH solution. In the latter case, the OH^- concentration, in large excess in the external solution, can be considered constant and the reaction rate becomes pseudo-first order. In the former case, the OH^- concentration decreases with the amount of lost ammonium groups, so that the reaction rate is proportional to the square of the IEC. The degradation rate should therefore increase with increasing IEC [28,60]. Indeed, the data in Fig. 11 show a larger ionic conductivity decrease for the samples with larger initial IEC.

The hydroxide reactivity increases significantly with decreasing hydration [16,28]. The general assumption is that no degradation occurs in water at least up to 80 °C. An estimation of the hydroxide concentration inside the membrane is possible using the water uptake WU, the IEC and the solution density d [26,61]:

$$[OH^-] = \frac{IEC \times d}{WU} \quad (6)$$

Taking as example Cl-PPO-TMA, the water uptake in pure water, WU = 0.26, and the IEC = 1.6 meq/g give $[OH^-] \approx 6$ mol/L assuming d = 1 g/cm^3. The water uptake measured in 2M NaOH is lower, WU = 0.10; similar observations were previously reported for PSU-TMA in various buffer solutions [62] and for SPEEK in salt solutions [63]. The degradation reaction takes therefore place in a medium with very high hydroxide concentration $[OH^-] \approx 16$ mol/L according to equation (6).

Assuming a reaction with the internal hydroxide ions, the reaction rate v can be written as a function of the square of the OH^- concentration:

$$v = k[OH^-]^2 = [OH^-]^2 \frac{k_B T}{h} e^{-\frac{\Delta G^{\ddagger}}{k_B T}} \quad (7)$$

In the Eyring equation, k_B is the Boltzmann constant, h the Planck constant, and T the absolute temperature.

According to equation (7), the increase of the reaction rate in 2 M NaOH in comparison with pure water would be seven-fold, if we consider the concentrations calculated above. Although it is well understood that the hydroxide activity must be considered at such high concentrations, this elementary calculation shows the large increase of reaction rate expected in 2 M NaOH.

The degradation kinetics are obviously also strongly dependent on the reaction temperature. One can calculate the ratio of the rate constants for two different temperatures using equation 8 and the activation energy (E_A = 27.0 kcal/mol) reported for an attack by OH^- ions solvated with 4 water molecules [28]. For a 6 M concentration, as in our case, the hydration number, λ, is around 9 in agreement with the data reported in 10 M NaOH (λ = 5) and 2 M NaOH (λ = 30) [16]; considering that the activation energy increases with decreasing λ [16], the above value is probably underestimated. Even so, a one order of magnitude lower rate constant is expected at 333 K, the usual temperature of operation of AEMFC, and the AEM should have an order of magnitude longer lifetime in presence of sufficient water. Indeed, published data at 333 K showed only 30% degradation of PPO with quaternary ammonium groups after 10 days in 1 M NaOH [42].

6. Conclusion

We performed a detailed analysis by various experimental techniques of the stability of anion exchange membranes based on PPO with grafted benzyl trimethylammonium groups anchored in different positions on the aromatic rings.

Contrasting results were obtained. From the point of view of the mechanical properties, the samples formed through the chloromethylation route showed the best results: the polymer was more ductile also after the aging treatment. The membranes prepared with the bromination strategy were fragile and difficult to manage. On the contrary, from the point of view of the resilience of the ionic conductivity, Br-PPO-TMA showed a better behavior.

The thermogravimetric analysis indicated that the chain scission by ether cleavage was an important degradation step together with the loss of ammonium groups confirmed by titration.

The nanophase separation, explored by SAXS, was lower for Br-PPO-TMA due to the hydrophobicity of residual Br in the aromatic ring.

In conclusion, the good mechanical properties of Cl-PPO-TMA before and after aging are a key point in the development of AEMFCs for non-stationary applications.

Declaration of competing interest

The authors declare that they have no known competing financial interests or personal relationships that could have appeared to influence the work reported in this paper.

Acknowledgments

The research leading to these results has received funding from the European Union's Horizon 2020 research and innovation programme under grant agreement CREATE No. 721065.

Appendix A. Supplementary data

Supplementary data to this article can be found online at https://doi.org/10.1016/j.polymer.2019.121931o.

References

[1] J.R. Varcoe, R.C.T. Slade, Prospects for alkaline anion-exchange membranes in low temperature fuel cells, Fuel Cells 5 (2) (2005) 187–200.
[2] J. Jagur-Grodzinski, Polymeric materials for fuel cells: concise review of recent studies, Polym. Adv. Technol. 18 (10) (2007) 785–799.
[3] G. Merle, M. Wessling, K. Nijmeijer, Anion exchange membranes for alkaline fuel cells: a review, J. Membr. Sci. 377 (1–2) (2011) 1–35.
[4] G. Couture, A. Alaaeddine, F. Boschet, B. Ameduri, Polymeric materials as anion-exchange membranes for alkaline fuel cells, Prog. Polym. Sci. 36 (11) (2011) 1521–1557.
[5] B. Bauer, H. Strathmann, F. Effenberger, Anion-exchange membranes with improved alkaline stability, Desalination 79 (2–3) (1990) 125–144.
[6] Z.F. Pan, L. An, T.S. Zhao, Z.K. Tang, Advances and challenges in alkaline anion exchange membrane fuel cells, Prog. Energy Combust. Sci. 66 (2018) 141–175.
[7] T. Palaniselvam, V. Kashyap, S.N. Bhange, J.B. Baek, S. Kurungot, Nanoporous graphene enriched with Fe/Co-N active sites as a promising oxygen reduction

electrocatalyst for anion exchange membrane fuel cells, Adv. Funct. Mater. 26 (13) (2016) 2150–2162.
[8] K.D. Kreuer, S.J. Paddison, E. Spohr, M. Schuster, Transport in proton conductors for fuel-cell applications: simulations, elementary reactions, and phenomenology, Chem. Rev. 104 (10) (2004) 4637–4678.
[9] P. Knauth, E. Sgreccia, A. Donnadio, M. Casciola, M.L. Di Vona, Water activity coefficient and proton mobility in hydrated acidic polymers, J. Electrochem. Soc. 158 (2) (2011) B159–B165.
[10] P. Knauth, M.L. Di Vona, Sulfonated aromatic ionomers: analysis of proton conductivity and proton mobility, Solid State Ion. 225 (2012) 255–259.
[11] M.G. Marino, J.P. Melchior, A. Wohlfarth, K.D. Kreuer, Hydroxide, halide and water transport in a model anion exchange membrane, J. Membr. Sci. 464 (2014) 61–71.
[12] Y. Pan, Q.D. Zhang, X.M. Yan, J.F. Liu, X.W. Xu, T.Y. Wang, I. El Hamouti, X. H. Ruan, C. Hao, G.H. He, Hydrophilic side chain assisting continuous ion-conducting channels for anion exchange membranes, J. Membr. Sci. 552 (2018) 286–294.
[13] J. Cheng, G.H. He, F.X. Zhang, A mini-review on anion exchange membranes for fuel cell applications: stability issue and addressing strategies, Int. J. Hydrogen Energy 40 (23) (2015) 7348–7360.
[14] M.A. Hickner, A.M. Herring, E.B. Coughlin, Anion exchange membranes: current status and moving forward, J. Polym. Sci. B Polym. Phys. 51 (24) (2013) 1727–1735.
[15] X. Chu, L. Liu, Y. Huang, M.D. Guiver, N. Li, Practical implementation of bis-six-membered N-cyclic quaternary ammonium cations in advanced anion exchange membranes for fuel cells: synthesis and durability, J. Membr. Sci. 578 (2019) 239–250.
[16] M.G. Marino, K.D. Kreuer, Alkaline stability of quaternary ammonium cations for alkaline fuel cell membranes and ionic liquids, Chemsuschem 8 (3) (2015) 513–523.
[17] J.J. Chen, C.P. Li, J.C. Wang, L. Li, Z.D. Wei, A general strategy to enhance the alkaline stability of anion exchange membranes, J. Mater. Chem. 5 (13) (2017) 6318–6327.
[18] Y. Ye, Y.A. Elabd, Chemical stability of anion exchange membranes for alkaline fuel cells, in: Polymers for Energy Storage and Delivery: Polyelectrolytes for Batteries and Fuel Cells, vol. 1096, American Chemical Society, 2012, pp. 233–251.
[19] A.D. Mohanty, S.E. Tignor, J.A. Krause, Y.-K. Choe, C. Bae, Systematic alkaline stability study of polymer backbones for anion exchange membrane applications, Macromolecules 49 (9) (2016) 3361–3372.
[20] J.Y. Jeon, S. Park, J. Han, S. Maurya, A.D. Mohanty, D. Tian, N. Saikia, M. A. Hickner, C.Y. Ryu, M.E. Tuckerman, S.J. Paddison, Y.S. Kim, C. Bae, Synthesis of aromatic anion exchange membranes by friedel-crafts bromoalkylation and cross-linking of polystyrene block copolymers, Macromolecules 52 (5) (2019) 2139–2147.
[21] M.L. Di Vona, R. Narducci, L. Pasquini, K. Pelzer, P. Knauth, Anion-conducting ionomers: study of type of functionalizing amine and macromolecular cross-linking, Int. J. Hydrogen Energy 39 (26) (2014) 14039–14049.
[22] R. Pizzoferrato, E. Ciotta, I.V. Ferrari, R. Narducci, L. Pasquini, A. Varone, M. Richetta, S. Antonaroli, M. Braglia, P. Knauth, M.L. Di Vona, Layered double hydroxides containing an ionic liquid: ionic conductivity and use in composite anion exchange membranes, Chemelectrochem 5 (19) (2018) 2781–2788.
[23] L. Pasquini, M.L. Di Vona, P. Knauth, Effects of anion substitution on hydration, ionic conductivity and mechanical properties of anion-exchange membranes, New J. Chem. 40 (4) (2016) 3671–3676.
[24] S. Gu, J. Skovgard, Y.S. Yan, Engineering the van der Waals interaction in cross-linking-free hydroxide exchange membranes for low swelling and high conductivity, Chemsuschem 5 (5) (2012) 843–848.
[25] M.L. Di Vona, M. Casciola, A. Donnadio, M. Nocchetti, L. Pasquini, R. Narducci, P. Knauth, Anionic conducting composite membranes based on aromatic polymer and layered double hydroxides, Int. J. Hydrogen Energy 42 (5) (2017) 3197–3205.
[26] L. Pasquini, F. Ziarelli, S. Viel, M.L. Di Vona, P. Knauth, Fluoride-ion-conducting polymers: ionic conductivity and fluoride ion diffusion coefficient in quaternized polysulfones, ChemPhysChem 16 (17) (2015) 3631–3636.
[27] M. Manohar, A.K. Das, V.K. Shahi, Alternative preparative route for efficient and stable anion-exchange membrane for water desalination by electrodialysis, Desalination 413 (2017) 101–108.
[28] D.R. Dekel, M. Arnar, S. Willdorf, M. Kosa, S. Dhara, C.E. Diesendruck, Effect of water on the stability of quaternary ammonium groups for anion exchange membrane fuel cell applications, Chem. Mater. 29 (10) (2017) 4425–4431.
[29] J. Yang, C. Liu, Y. Hao, X. He, R. He, Preparation and investigation of various imidazolium-functionalized poly(2,6-dimethyl-1,4-phenylene oxide) anion exchange membranes, Electrochim. Acta 207 (2016) 112–119.
[30] A. Katzfuss, V. Gogel, L. Jorissen, J. Kerres, The application of covalently cross-linked BrPPO as AEM in alkaline DMFC, J. Membr. Sci. 425 (2013) 131–140.
[31] F.L.K. Greenwood, M.D.J. Sedlak, 4-Bromo-2-heptene. Organic syntheses, Collec. Vol. Sci. Pap. 4 (1963) 108.
[32] M.L. Di Vona, G. Alberti, E. Sgreccia, M. Casciola, P. Knauth, High performance sulfonated aromatic ionomers by solvothermal macromolecular synthesis, Int. J. Hydrogen Energy 37 (10) (2012) 8672–8680.
[33] G. Gebel, Structure of membranes for fuel cells: SANS and SAXS analyses of sulfonated PEEK membranes and solutions, Macromolecules 46 (15) (2013) 6057–6066.
[34] K.D. Kreuer, G. Portale, A critical revision of the nano-morphology of proton conducting ionomers and polyelectrolytes for fuel cell applications, Adv. Funct. Mater. 23 (43) (2013) 5390–5397.
[35] H. Mendil-Jakani, I.Z. Lopez, P.M. Legrand, V.H. Mareau, L. Gonon, A new interpretation of SAXS peaks in sulfonated poly(ether ether ketone) (sPEEK) membranes for fuel cells, Phys. Chem. Chem. Phys. 16 (23) (2014) 11228–11235.
[36] H.S. Dang, P. Jannasch, A comparative study of anion-exchange membranes tethered with different hetero-cycloaliphatic quaternary ammonium hydroxides, J. Mater. Chem. 5 (41) (2017) 21965–21978.
[37] K. Vezzu, A.M. Maes, F. Bertasi, A.R. Motz, T.H. Tsai, E.B. Coughlin, A.M. Herring, V. Di Noto, Interplay between hydroxyl density and relaxations in poly (vinylbenzyltrimethylammonium)-b-poly(methylbutylene) membranes for electrochemical applications, J. Am. Chem. Soc. 140 (4) (2018) 1372–1384.
[38] D. Marx, A. Chandra, M.E. Tuckerman, Aqueous basic solutions: hydroxide solvation, structural diffusion, and comparison to the hydrated proton, Chem. Rev. 110 (4) (2010) 2174–2216.
[39] J. Jachowicz, M. Kryszewski, P. Kowalski, Thermal-degradation of poly(2,6-dimethyl-1,4-phenylene oxide).1 Mechanism of degradation, J. Appl. Polym. Sci. 22 (10) (1978) 2891–2899.
[40] R.P. Singh, Thermal-degradation and stabilization of poly(2,6-dimethyl-1,4-phenylene oxide), Eur. Polym. J. 18 (2) (1982) 117–122.
[41] D.L. Vien, The Handbook of Infrared and Raman Frequencies of Organic Molecules, Academic Press, Inc., San Diego, 1992.
[42] C.G. Arges, L. Wang, M.-s. Jung, V. Ramani, Mechanically stable poly(arylene ether) anion exchange membranes prepared from commercially available polymers for alkaline electrochemical devices, J. Electrochem. Soc. 162 (7) (2015) F686–F693.
[43] J.F. Zhou, M. Unlu, J.A. Vega, P.A. Kohl, Anionic polysulfone ionomers and membranes containing fluorenyl groups for anionic fuel cells, J. Power Sources 190 (2) (2009) 285–292.
[44] G.F.L. Ehlers, K.R. Fisch, W.R. Powell, Thermal degradation of polymers with phenylene units in the chain. I. Polyphenylenes and poly(phenylene oxides), J. Polym. Sci. A 1 Polym. Chem. 7 (10) (1969) 2931–2953.
[45] C.G. Arges, L.H. Wang, J. Parrondo, V. Ramani, Best practices for investigating anion exchange membrane suitability for alkaline electrochemical devices: case study using quaternary ammonium poly(2,6-dimethyl 1,4-phenylene)oxide anion exchange membranes, J. Electrochem. Soc. 160 (11) (2013) F1258–F1274.
[46] M. Zhang, J.L. Liu, Y.G. Wang, L.A. An, M.D. Guiver, N.W. Li, Highly stable anion exchange membranes based on quaternized polypropylene, J. Mater. Chem. 3 (23) (2015) 12284–12296.
[47] M. Tanaka, M. Koike, K. Miyatake, M. Watanabe, Synthesis and properties of anion conductive ionomers containing fluorenyl groups for alkaline fuel cell applications, Polym. Chem. 2 (1) (2011) 99–106.
[48] X.G. Li, High-resolution thermogravimetry of poly(2,6-dimethyl-1,4-phenylene oxide), J. Appl. Polym. Sci. 71 (11) (1999) 1887–1892.
[49] H.S. Dang, P. Jannasch, Exploring different cationic alkyl side chain designs for enhanced alkaline stability and hydroxide ion conductivity of anion-exchange membranes, Macromolecules 48 (16) (2015) 5742–5751.
[50] R.C. Bopp, U. Gaur, R.P. Kambour, B. Wunderlich, Effect of bromination on the thermal-properties of poly(2,6-dimethyl-1,4-phenylene oxide), J. Therm. Anal. 25 (2) (1982) 243–258.
[51] S.H. Goh, S.Y. Lee, Thermal-stability of bromobenzylated poly(2,6-dimethyl-1,4-phenylene oxide), Thermochim. Acta 120 (1987) 293–298.
[52] J. Parrondo, Z.Y. Wang, M.S.J. Jung, V. Ramani, Reactive oxygen species accelerate degradation of anion exchange membranes based on polyphenylene oxide in alkaline environments, Phys. Chem. Chem. Phys. 18 (29) (2016) 19705–19712.
[53] M. Liang, Poly(phenylene oxide) 3 (2011).
[54] C.G. Arges, V. Ramani, Two-dimensional NMR spectroscopy reveals cation-triggered backbone degradation in polysulfone-based anion exchange membranes, Proc. Natl. Acad. Sci. U.S.A. 110 (7) (2013) 2490–2495.
[55] S. Chempath, B.R. Einsla, L.R. Pratt, C.S. Macomber, J.M. Boncella, J.A. Rau, B. S. Pivovar, Mechanism of tetraalkylammonium headgroup degradation in alkaline fuel cell membranes, J. Phys. Chem. C 112 (9) (2008) 3179–3182.
[56] S. Chempath, J.M. Boncella, L.R. Pratt, N. Henson, B.S. Pivovar, Density functional theory study of degradation of tetraalkylammonium hydroxides, J. Phys. Chem. C 114 (27) (2010) 11977–11983.
[57] H. Long, K. Kim, B.S. Pivovar, Hydroxide degradation pathways for substituted trimethylammonium cations: a DFT study, J. Phys. Chem. C 116 (17) (2012) 9419–9426.
[58] Y.K. Choe, C. Fujimoto, K.S. Lee, L.T. Dalton, K. Ayers, N.J. Henson, Y.S. Kim, Alkaline stability of benzyl trimethyl ammonium functionalized polyaromatics: a computational and experimental study, Chem. Mater. 26 (19) (2014) 5675–5682.
[59] M.J. Frisch, et al., Gaussian 16, Revision C.01, Gaussian, Inc., Wallingford, CT, 2016.
[60] V.J. Bharath, R. Jervis, J. Millichamp, T.P. Neville, T. Mason, B. Tjaden, P. R. Shearing, R.J.C. Brown, G. Manos, D.J.L. Brett, Alkaline anion exchange membrane degradation as a function of humidity measured using the quartz crystal microbalance, Int. J. Hydrogen Energy 42 (9) (2017) 6243–6249.
[61] M.L. Di Vona, L. Pasquini, R. Narducci, K. Pelzer, A. Donnadio, M. Casciola, P. Knauth, Cross-linked sulfonated aromatic ionomers via SO2 bridges: conductivity properties, J. Power Sources 243 (2013) 488–493.
[62] L. Pasquini, O. Wacrenier, M.L.D. Vona, P. Knauth, Hydration and ionic conductivity of model cation and anion-conducting ionomers in buffer solutions (phosphate, acetate, citrate), J. Phys. Chem. B 122 (50) (2018) 12009–12016.
[63] R. Narducci, M.L. Di Vona, P. Knauth, Cation-conducting ionomers made by ion exchange of sulfonated poly-ether-ether-ketone: hydration, mechanical and thermal properties and ionic conductivity, J. Membr. Sci. 465 (2014) 185–192.